Adv. Polar Upper Atmos. Res., **19**, 106–134, 2005

Review

Inner magnetospheric plasma interactions and coupling with the ionosphere

Mei-Ching Fok[1]*, Yusuke Ebihara[2] and Thomas E. Moore[1]

[1]*NASA Goddard Space Flight Center, Greenbelt, Maryland 20771, U.S.A.*
[2]*National Institute of Polar Research, Kaga 1-chome, Itabashi-ku, Tokyo 173-8515*
**Corresponding author. E-mail: mei-ching.h.fok@nasa.gov*

(Received March 18, 2005; Accepted June 13, 2005)

Abstract: The inner magnetosphere occupies a vast volume in space containing a relatively low-density mixture of hot and cold plasmas: the ring current, plasmasphere and radiation belt. Energy is transferred from the ring current to the cold plasmas through Coulomb collisions and wave-particle interactions, producing temperature enhancements in the plasmasphere. The plasma waves generated in the plasmasphere cause pitch-angle and energy diffusion of the energetic particles. The magnetic disturbances generated from the ring current alter the drift paths of radiation belt particles, causing radiation belt flux dropout during magnetic storm main phases. The ionosphere is filled with dense and cold plasmas in a 1000-km-thick shell above the Earth's surface at ~100 km altitude. Despite the distinct differences in size, location and physical properties, the ionosphere and the inner magnetosphere are tightly connected to each other. The ionosphere is an important source of magnetospheric ions. Energy transported down from the inner magnetosphere to the ionosphere produces observable temperature enhancements and optical emissions in the ionosphere. The electric coupling between the ionosphere and magnetosphere explains features such as shielding field, non-linear response of the ring current to the plasma-sheet source, and the post-midnight enhancement of the storm-time ring current flux. Even though many signatures are well described from the perspective of magnetosphere-ionosphere coupling, there are still unanswered questions, for example, the precise roles of wave-particle interactions in ring current loss and plasmaspheric heating, the cause of rapid storm initial recovery, the source of O^+ enhancement at substorm expansion, and the causes of outer radiation belt enhancement during storm recovery. The unresolved questions can be answered through careful cross analysis of the observational data from the ongoing and future imaging and multi-point missions with simulation results of large-scale modeling.

key words: inner magnetosphere, hot-cold interactions, magnetosphere-ionosphere coupling

1. Introduction

The ionosphere is a region in the upper atmosphere (~100–1000 km altitude) that consists of significant amount of cold (<1 eV) ions and electrons (Comfort *et al.*,

1985), which are produced through ionizations of the neutral atmosphere by solar radiations and collisions with energetic particles (Schunk and Nagy, 2000). Plasma drifts in the ionosphere are determined by the electric field impressed by magnetospheric plasma motions and local collision frequencies. In the topside ionosphere where collisions are negligible, electrons and ions basically execute $E \times B$ drift. At lower altitudes where collisions are significant, plasma drift velocity is inclined at an angle of $\tan^{-1}(\nu/\omega)$, where ν and ω are collision and cyclotron frequencies, respectively. In the ionosphere, currents flow according to the Ohm's law with conductivity tensor consisting Hall, Pedersen and Cowling conductivities. Electric field can be expressed as negative gradient of a potential since magnetic field is basically constant with time in the ionosphere.

The inner magnetosphere consists of plasma populations that vary widely in characteristics, *i.e.*, the plasmasphere, ring current and the radiation belt (Wolf, 1995). The plasmasphere is basically the outward extension of the ionosphere. It is often outlined by a sharp boundary called the plasmapause, which separates the corotating dense region from the low-density exterior. The size and shape of the plasmasphere is largely controlled by the convection electric field reflecting global magnetospheric plasma circulation. During quiet periods, the plasmasphere has a tear-drop shape with the tip located around dusk local time. During active times, strong convection sweeps the plasmas toward dayside and forms an elongated extension of the plasmasphere known as plasma plume (or less precisely, tail) (Grebowsky, 1970; Grebowsky and Chen, 1976). Almost forty years since the discovery of the plasmapause (Carpenter, 1963), all our knowledge about the plasmasphere dynamics and configuration came from theoretical studies, ground-based or *in-situ* measurements. With the launch of the Imager for Magnetopause-to-Aurora Global Exploration (IMAGE) mission in 2000 (Burch, 2000), the global structures of the plasmasphere were finally revealed through the EUV images of the region (Sandel *et al*., 2001). The predicted development of plasma plumes was confirmed and new features such as plasmasphere 'shoulders' and 'voids' were discovered (Burch *et al*., 2001).

The ring current is a population of energetic ($\sim 1-300$ keV) ions and electrons flowing in the inner magnetosphere in the range of L shells from ~2 to 8. Major ion species in the ring current are H^+, O^+, He^+, N^+ and He^{++} (Gloeckler and Hamilton, 1987; Daglis *et al*., 1993). During active periods, enhanced ring current fluxes produce worldwide perturbations to the surface magnetic field, which are used to identify magnetic storms (Daglis, 2003). The ring current contains plasmas from the solar wind and ionosphere. Ring current H^+ is supplied from the solar wind and ionosphere, while O^+, He^+ and N^+ are mainly from the ionosphere, and He^{++} is from the solar wind. Solar wind plasmas enter the ring current region primarily *via* the flanks, and to a less extend through the cusp and plasma sheet. Ionospheric particles enter the inner magnetosphere predominantly through the plasma sheet and then convect earthward to the ring current region (Moore *et al*., 2005a). During storm main phase of strong convection, the ring current is highly asymmetric and peaks on the nightside (Stüdemann *et al*., 1987; Ebihara *et al*., 2002). When the convection strength subsides, the ring current becomes more symmetric in local time as more particles are drifting in closed paths (Liemohn *et al*., 1999; Pollock *et al*., 2001; Ebihara *et al*., 2002). An

in-depth and comprehensive discussion on the ring current sources, buildup and decay can be found in the excellent review by Daglis *et al.* (1999).

Explorer I and III in 1958 revealed the existence of energetic electrons and protons (up to MeV's for electrons and tens of MeV for protons) trapped in the magnetosphere, later named as the Van Allen radiation belt (Van Allen, 1959). Since its discovery, the radiation belt has been a subject of active research owning to its scientific significance and its impacts to space borne electronic systems and humans in space. The radiation belt populates about the same region as the ring current. Particles in the radiation belt are believed to originate from the solar wind, ionosphere and cosmic ray albedo (Walt, 1996; Baker *et al*., 1996). During geomagnetic active periods, the intensities of radiation belt particles vary significantly. A flux decrease is often seen during the main phase of a magnetic storm, the signature that is known as the "Dst effect". When a storm intensifies, the magnetic field produced by the ring current inflates the main field. The drift shells of energetic particle in the radiation belt expand outward correspondingly (conversation of the third adiabatic invariant) and particles decelerate (Dessler and Karplus, 1961; Kim and Chen, 1997). This de-energization causes a decrease in particle fluxes since the energy spectrum slope is usually negative in the radiation belt energy range. During the storm recovery, the radiation belt fluxes recover as well, to a level higher than, equal to, or lower than the pre-storm intensity, seeming to depend on the solar wind velocity (Reeves *et al*., 2003). The radiation belt is also be greatly enhanced when the magnetosphere is compressed by interplanetary shocks (Blake *et al*., 1992; Hudson *et al*., 1996).

The hot and cold plasma populations in the inner magnetosphere interact with each other. Energy transfer between the ring current and the plasmasphere causes decay of the hot population and heating in the cold plasmasphere (Kozyra *et al*., 1987; Fok *et al*., 1993). Anisotropies in ring current and radiation belt particles excite plasma wave growth in the plasmasphere. These waves, in turn, give rise to pitch-angle and energy diffusion of the energetic plasmas (Jordanova *et al*., 2001; Khazanov *et al*., 2003b; Tsurutani and Smith, 1977; Summer *et al*., 1998). Wave-particle interactions are thus important mechanisms in ring current and radiation belt decay and buildup. The magnetic field produced by the ring current alters the drift paths of radiation belt particles causing reversible (adiabatic) changes or irreversible losses of the radiation belt (Kim and Chan, 1997).

Despite distinct differences in size, location and physical properties, the ionosphere and the magnetosphere are tightly connected to each other through magnetic field lines (Wolf, 1975; Khazanov *et al*., 2003a). Variations and disturbances that occur on one side will induce corresponding changes on the other side (Schulz, 1997). Certain features observed in the magnetosphere cannot be understood without examining the contribution from the ionosphere, and vice versa. Likewise, some interactions between magnetospheric plasma populations have to be linked through the ionosphere. For instance, asymmetries in the ring current particle pressure tensor produce field aligned currents flowing into and out from the ionosphere. These currents control the ionospheric electric potential distributions and couple plasma convection in both the ionosphere and magnetospheric plasmas (Harel *et al*., 1981; Wolf, 1983). Another crucial element in determining the convection pattern is the ionosphere conductivity

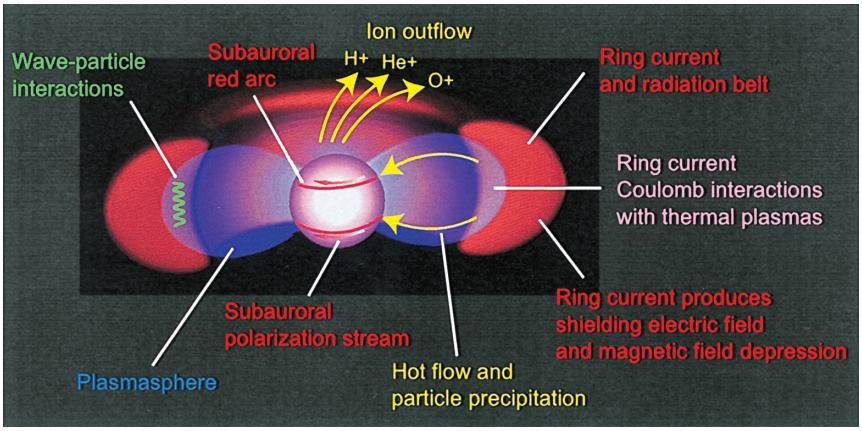

Fig. 1. Cartoon sketch shows major interactions between plasmas in the inner magnetosphere and coupling with the ionosphere.

(Wolf, 1970; Ebihara *et al*., 2004), which is strongly moderated by precipitation of magnetospheric electrons and ions. In addition to electric coupling, the ionosphere also serves as a source (Daglis and Axford, 1996) and a sink to the magnetospheric plasmas. Figure 1 summarizes the major processes coupling plasmas in the inner magnetosphere and ionosphere. In this paper, we review the progress in understanding the interactions between magnetospheric plasmas and coupling with the ionosphere. We then conclude with questions that need further investigation.

2. Magnetospheric plasma interactions

2.1. hot-cold interactions through Coulomb collisions

In this paper, hot-cold interactions refer to coupling between the ring current (hot) and the plasmasphere (cold) particles. In the region of overlap between the ring current and the plasmasphere, the two plasma populations interact with each other *via* Coulomb collisions. Strong interactions especially occur between cold plasmasphere electrons and hot ring current ions due to their comparable velocities (Fok *et al*., 1991a). Energy is transferred from the hot ions to the plasmaspheric particles. The hot ions thus lose energy and when their energies are reduced to below the ring current energy range (< 1 keV), these ions are treated as lost from the ring current. The hot ions also suffer angular deflection but the effect is minimal (Wentworth *et al*., 1959). Coulomb interaction with the plasmasphere is one of the major loss mechanisms for ring current ions other than charge exchange loss. In fact, at low energies, Coulomb loss are often dominant over charge exchange loss. Figure 2 (taken from Fok *et al*., 1991a) shows a comparison of Coulomb decay lifetimes with charge exchange lifetimes for ring current H^+, He^+ and O^+. As shown in the figure, Coulomb lifetimes are often shorter than charge exchange lifetimes for ring current H^+ below a few keV, for He^+ and O^+ below tens of keV. Jordanova *et al.* (1998) simulated the ring current development during the storm on October 18–26, 1995. They found Coulomb collisions to be the second

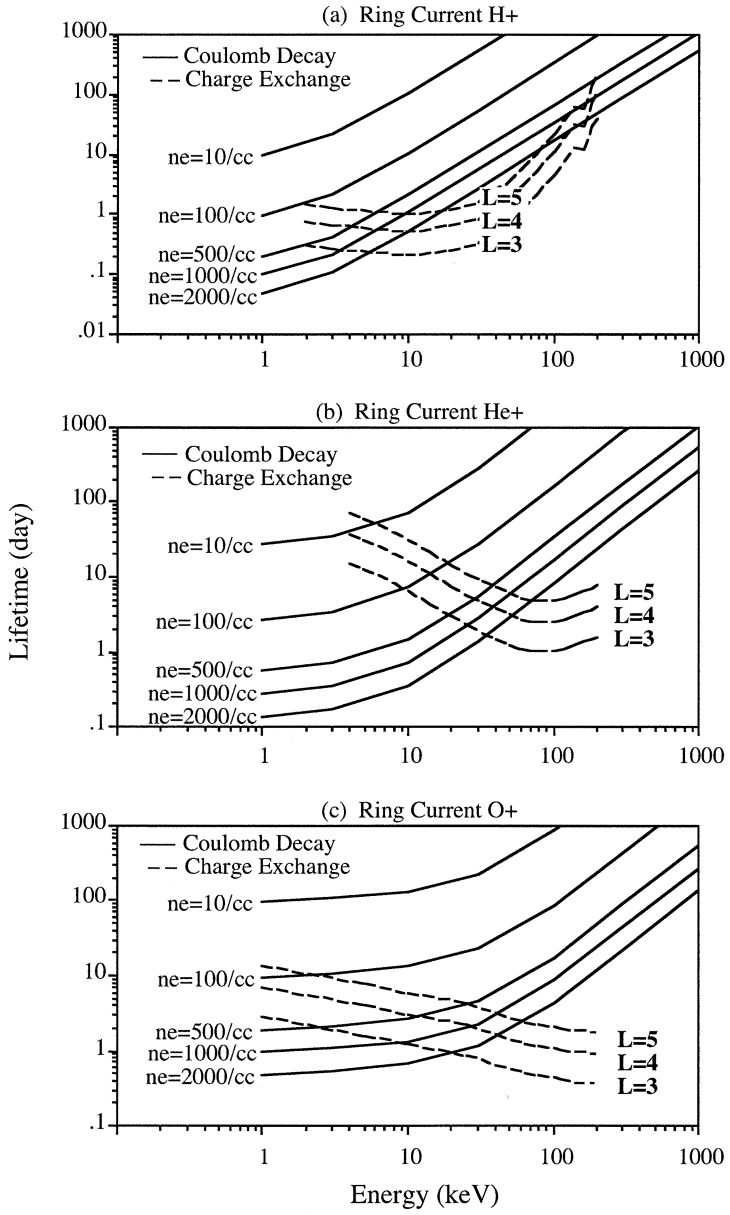

Fig. 2. Comparison of Coulomb decay lifetimes (solid lines) with charge exchange lifetimes (dashed lines) for ring current H^+ (top panel), He^+ (middle panel), and O^+ (bottom panel). Coulomb decay lifetimes are calculated using plasmasphere density (ne) = 2000, 1000, 500, 100, and 10 cm^{-3} (taken from Fok et al., 1991a).

important loss process, followed the charge exchange loss.

As mentioned above, Coulomb drag from cold plasmas causes energy degradation in the ring current. In a simulation study, Fok *et al.* (1993) found a population of

low-energy (10–500 eV) ions is intensified during the storm recovery at $L=2$–4. Enhanced 10–500 eV fluxes of H^+, He^+ and O^+ were developed a few hours into the recovery phase. After 2 days of recovery, the low-energy H^+ flux decreases in an order of magnitude. In contrast, there is an order of magnitude increase in the low-energy O^+ flux with the peak flux located at $L=2$–3. Fok *et al.* (1993) confirmed that these low-energy ions are not injected from the nightside but generated locally from energy degradation of ring current ions. The different times of appearance for H^+ and O^+ low-energy fluxes can be accounted for by their different Coulomb decay lifetimes. Ring current H^+ of energies of 1–10 keV lose their energies to the plasmasphere faster than ring current O^+ of the same energy range. After the low-energy (10–500 eV) H^+ is built up, they lose energy to below 10 eV in a few more hours due to continued Coulomb drag from the plasmasphere. The Coulomb lifetime for ring current O^+ is longer, so it takes ~1 day for low-energy O^+ to develop and the high flux lasts for a few days. Kistler *et al.* (1989) calculated the ring current ion fluxes during the storm on 19 September 1984, considering ion drifts and charge exchange loss. The simulated H^+ flux at $L=3$–4 at storm early recovery was compared with the CCE/CHEM measurement. They found very good agreements except below 5 keV. Their model underestimated the H^+ flux at low energies. We suspect this discrepancy came from the exclusion of low-energy ion buildup due to Coulomb collisions between ring current ions and the plasmasphere. A buildup of suprathermal ions was also observed by Shelley *et al.* (1985) during the storm main phase and recovery on 4 September 1984. The temporal and spatial distributions of this observed suprathermal ions are consistent with the theoretical calculation by Fok *et al.* (1993) as presented above.

While the hot ring current ions are degraded in energy when they have Coulomb collisions with the plasmasphere, the energy transfer from the hot ions to the cold plasmas will cause high electron and ion temperatures in the plasmasphere if no compensating loses occur. No electron temperature measurement in the plasmasphere has been made because of technical difficulties. However, enhanced plasmaspheric ion temperatures were observed during magnetic active times by the Retarding Ion Mass Spectrometer (RIMS) on Dynamics Explorer 1 (DE 1) (Comfort *et al*., 1988). Fok *et al.* (1995) calculated the plasmaspheric ion temperature during the recovery phase of the magnetic storm on 6–11 February 1986 using the Field Line Interhemispheric Plasma (FLIP) model, taking into account the additional heat source from the ring current. Figure 3 shows the calculated altitude profiles of ion temperature at different times in storm recovery at $L=4$, 0900 LT (left panel) and 2200 LT (right panel). The figure shows that the ion temperature does not change with time if there is no heating from the ring current. However, with the additional magnetospheric heat source, ion temperatures above 500 km increase rapidly in the early recovery phase and then gradually return toward the quiet-time level. For comparison, the mean DE-1/RIMS H^+ temperatures during October and November of 1981 (Comfort *et al*., 1988) are also shown. Both high and low altitude data on the morning side are shown and only the high altitude measurement is plotted on the evening side. It is clearly seen in the figure that the observed high ion temperature cannot be explained without additional heat input from the magnetosphere.

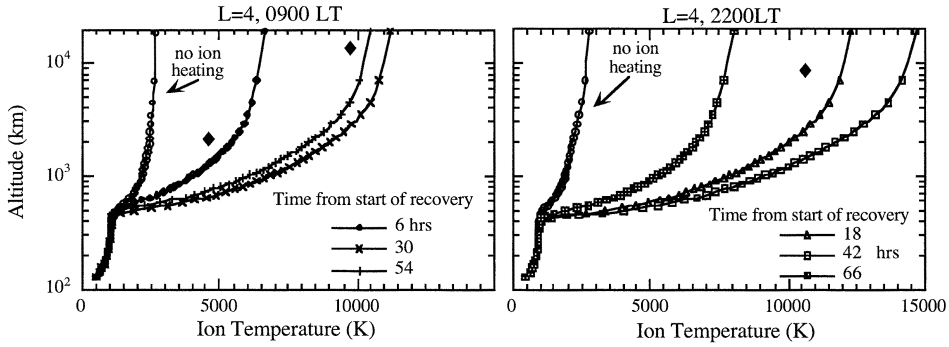

Fig. 3. Calculated altitude profiles of ion temperature at L=4 on the morning side (left) and evening (right). Average DE-1/RIMS data in October to November 1981 are shown with the ◆ (taken from Fok et al., 1995).

2.2. Magnetospheric plasma interactions through waves

Three kinds of plasma wave will be discussed: electromagnetic ion cyclotron (EMIC) waves, whistler mode chorus, and plasmaspheric hiss. These waves are generated in the inner magnetosphere and serve as channels for transferring energy from one plasma population to the others. They are important in plasmasphere heating, ring current-radiation belt loss and buildup.

2.2.1. EMIC Waves

EMIC waves are left-hand polarized with frequencies near ion cyclotron frequencies. EMIC waves propagate along magnetic field lines, reflecting at the ionosphere and bouncing between conjugate ionospheric points. Ion cyclotron modes grow when the ring current ion pitch-angle distribution is sufficiently anisotropic, with more energy perpendicular than parallel to the magnetic field (Kennel and Petschek, 1966). Magnetospheric processes such as convection, Coulomb and charge exchange interactions tend to reduce the field-parallel flux of ring current ions, providing the free energy for EMIC wave excitations. The amplification of EMIC waves also depends on the cold plasma density. Near the plasmapause where the density gradient is steep, EMIC waves bounce several times across the equator and thus experience multiple wave gains (Thorne and Horne, 1992). EMIC waves have been observed in the inner magnetosphere, especially in the vicinity of the plasmapause (Anderson *et al*., 1992; Fraser *et al*., 1992, 1996). The occurrence and intensity of EMIC waves are much higher during storms than quiet times (Fraser *et al*., 1992; Erlandson and Ukhorskiy, 2001). The active wave regions move to lower latitudes as storm develops (Braysy *et al*., 1998), along with the storm time plasmas.

EMIC waves cause pitch-angle diffusions and eventually precipitation losses of ring current ions. Jordanova *et al.* (2001) simulated the ring current ion fluxes during the 14–16 May 1997 storm, including losses due to wave-particle interactions. They found the global patterns of proton precipitation moved to lower L shells during storm main phase and receded back toward larger L shells in storm recovery, consistent with the EMIC wave observations mentioned above (Braysy *et al*., 1998). Kozyra *et al.* (1997a) studied the contribution of EMIC wave-induced precipitation to ring current decay

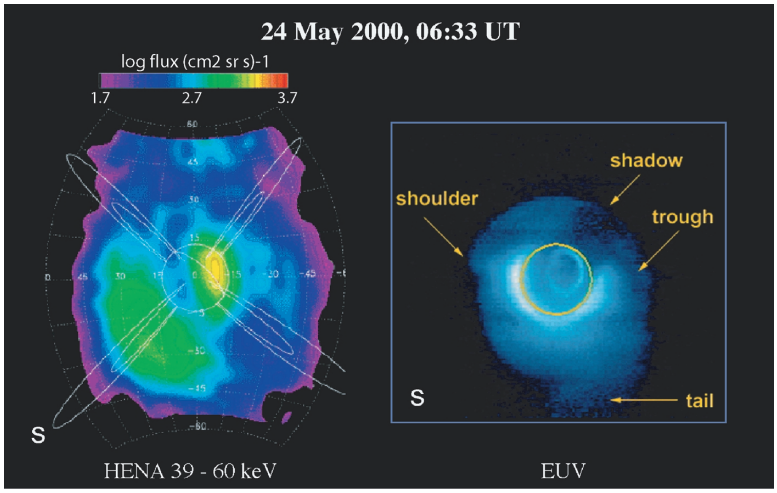

Fig. 4. IMAGE HENA (left) and EUV (right) images at 0633 UT on 24 May 2000. "S" represents the sun direction in both panels.

during the storm on 2–6 November 1993. They found an additional ~8 nT recovery in the Dst index. Since the launch of the IMAGE spacecraft in 2000, simultaneous images of the ring current and the plasmasphere have been obtained. To illustrate the advantage of multiple imaging, the left panel of Fig. 4 shows the ring current ion image from the High Energy Neutral Atom (HENA) imager (Mitchell *et al*., 2000) on IMAGE taken at 0633 UT on 24 May 2000. Dipole field lines of $L = 4$ and 8 at 4 local times are overlaid. The Sun direction is indicated by an "S". As shown in the figure, ENA flux peaks around noon at high altitude. At low altitude another peak is found in the dusk-midnight sector as a result of ring current precipitation. The right panel is the image of the plasmasphere taken at the same time from the Extreme Ultraviolet (EUV) imager (Sandel *et al*., 2000). The EUV image is orientated the same as the ENA image. The dark area in the anti-sunward direction is the shadow of the Earth. Features such as plasmaspheric tail, shoulder and trough are clearly seen in the EUV image. As shown in Fig. 4, the plasmasphere bulge-tail collocates with the high altitude trough in ENA flux at dusk. It is possible that strong EMIC waves in the bulge region deplete ring current ions by scattering them into the loss cone and causing strong precipitation at low altitude (Burch *et al*., 2001).

Radiation belt electrons also interact with EMIC waves through cyclotron resonance. Using balloon-borne X-ray detectors, Lorentzen *et al.* (2000) found intense X-ray event associated with atmospheric bremsstrahlung from 1.7 MeV precipitation electrons during a substorm. They interpreted the event as electron pitch-angle scattering and precipitation caused by resonance with EMIC waves. Based on quasi-linear theory, Summers and Thorne (2003) calculated the electron pitch-angle diffusion coefficients for cyclotron resonance with EMIC waves. They found, under typical storm condition in the duskside plasmasphere, only electrons with energy above 1 MeV to be resonant with EMIC waves. The time scale for removing these energetic

electrons by EMIC wave scattering during magnetic storms is as short as several hours to one day. The location of the calculated precipitation is consistent with the observation by Lorentzen *et al.* (2000).

EMIC waves resonant with ring current ions and radiation belt electrons cause precipitation losses of energetic particles. On the other hand, these waves are sources of heating to thermal electrons as they go through Landau damping. The ion cyclotron phase velocity, essentially the Alfvén speed, is comparable to the thermal velocity of plasmaspheric electrons. This suggests that Landau resonance with the thermal electrons is important. Since more electrons are moving slower than the wave phase velocity than those are moving faster, EMIC waves are damped and thermal electrons are heated by the waves. Cornwall *et al.* (1971) estimated the energy absorbed by plasmasphere electrons through Landau damping of EMIC waves. Together with energy deposition from Coulomb interactions with ring current ions, they found the combined heat flux to the ionosphere is sufficient to drive the stable aurora red (SAR) arcs in the ionosphere to observable intensities. Gorbachev *et al.* (1992) calculated the wave energy transfer to the thermal plasmas by means of Landau damping. The heat flux to electrons was found to be $\sim 3 \times 10^{10}$ eV cm^{-2}s^{-1} and 4×10^{8} eV cm^{-2}s^{-1} for ions. The predicted plasmaspheric temperatures with this additional heat source agreed well with observations for various satellites. This is an excellent example demonstrating that EMIC waves serve as media for energy transfer from hot plasmas to the cold plasmasphere. The hot plasmas provide the free energy for wave generation and the subsequent damping of these waves heats up the cold plasmas.

2.2.2. Whistler mode chorus

Whistler mode waves are right-hand polarized with frequencies less than the electron gyro-frequency. They travel along magnetic field lines or are refracted across field lines. Whistler mode chorus is identified as quasi-periodic, series of overlapping rising and falling tones (Shawhan, 1979). Two separated chorus emissions were observed in two distinct regions: high-latitude and low-latitude magnetosphere (Tsurutani and Smith, 1977; Meredith *et al*., 2001). Both studies found the high-latitude chorus is principally on the dayside. The low-latitude chorus was observed mostly outside the plasmasphere at all local times but predominantly in the post-midnight to dayside magnetosphere. A close relationship between substorm activities and the low-latitude chorus is found and it is suggested that these chorus emissions are generated by injection of 10–100 keV electrons (Tsurutani and Smith, 1977; Isenberg *et al*., 1982; Meredith *et al*., 2001). As substorm ring current electrons are injected on the nightside, they gradient-curvature drift to the dayside through dawn. During their earthward transport, the electrons are energized preferentially in the perpendicular direction. The resulting anisotropy in perpendicular and parallel electron temperatures generates instability or excitation of whistler mode chorus.

Whistler mode chorus cause energy and pitch-angle diffusion of radiation belt electrons. During the recovery phases of magnetic storms, the fluxes of outer belt electrons are often seen to increase, exceeding the pre-storm level (Reeves *et al*., 2003). Two types of mechanism are suggested to be responsible for this storm-time enhancement: earthward diffusion of injected particles from the plasma sheet and internal energization processes. Green and Kivelson (2004) examined the radial profiles of

electron phase space density using data from the Polar High Sensitivity Telescope energetic detector. They concluded that their results are best explained by an internal acceleration process at $L \sim 5$. Energy diffusion due to interaction with the whistler mode chorus is the most accepted candidate for this energization process. Summers and Ma (2000) developed a kinetic (Fokker-Planck) model of relativistic electrons, considering energy diffusion based on gyroresonance electron-whistler mode waves and precipitation due to pitch-angle scattering by EMIC and whistler mode waves. They assumed a constant background plasma density and whistler amplitudes on the order of 100 pT. Their model is able to generate the observable increases in relativistic electrons during storm recovery phases. On the other hand, MeV electrons experience pitch-angle scattering when interact with the whistler mode chorus and precipitate into the atmosphere. This diffusion loss is evident in the collocation of observed chorus emissions and MeV electron microburst precipitation (O'brien *et al*., 2003).

2.2.3. Plasmaspheric hiss

Another type of whistler mode turbulence propagates in the magnetosphere is the plasmaspheric hiss. These waves have the same frequency range (100 Hz–5 kHz) as the chorus. However, plasmasphere hiss emissions are mostly seen inside the plasmapause and for this reason they are named. Plasmaspheric hiss is relatively steady, persistently seen throughout the plasmasphere. It is proposed that plasmaspheric hiss is generated through cyclotron resonant instability with 10–100 keV electrons that diffuse inward to the plasmasphere from the outer belt (Thorne *et al*., 1973; Shawhan, 1979). The generation region is presumed to lie in the outer plasmasphere. From the source, waves propagate to fill the plasmasphere (Lyons *et al*., 1972). However, ray-tracing and growth rate calculation carried out by Huang *et al.* (1983) produced significantly lower wave intensity than observed hiss emissions, suggesting that wave sources other than anisotropic electron cyclotron resonance are needed to inject sufficient wave energy in the outer plasmasphere (Church and Thorne, 1983). Lightning is another possible source of plasmaspheric hiss. Lightning generates a broad electromagnetic wave spectrum in the lower ionosphere. These wave transmit through the ionosphere into the plasmasphere and experience dispersion as they propagate. Using data from DE 1 satellite, Sonwalkar and Inan (1989) observed close relation between lightning and hiss emission. They suggested that lightning-generated whistler is an important embryonic source for VLF hiss. Recent work by Green *et al.* (2005) also supports that lightning is the dominant source for plasmaspheric hiss.

Whistler mode plasmaspheric hiss is believed to be the source of the slot region that separates the inner and outer radiation belts during quiet periods. Plasmaspheric hiss interacts with radiation belt electrons through gyroresonance, causing pitch-angle diffusion and subsequent precipitation loss of these energetic electrons. The slot region is located at L shells ~2–3.5, where precipitation decay rates are comparatively high and radial diffusion is weak to balance the loss. Lyons *et al.* (1972) computed the pitch-angle diffusion coefficients of energetic electrons due to interaction with plasmaspheric hiss and solve the diffusion equation of electron distribution function. In their calculation, they considered cyclotron-harmonic and Landau resonances, as well as oblique propagation of waves. Their calculated pitch-angle distribution and precipitation lifetimes are in good agreement with satellite observations. Albert (1994) extended the

calculation of Lyon *et al.* (1972) by considering more harmonics, but in an efficient way such that the computation is still manageable. They found the improved precipitation lifetimes for electron energies above 500 keV and L shells greater than 3 are shorter than those previously reported by Lyon *et al.* (1972).

As mentioned above, plasmaspheric hiss emissions are generated in the lower ionosphere by lightning and probably further excited by the ring current electrons. On the other hand, part of the hiss wave energy is damped by the ring current and radiation belt ions. Kozyra *et al.* (1994, 1995) calculated the energy, pitch-angle and cross diffusion coefficients of energetic (≥ 80 keV) ions when they undergo resonant interactions with the ducted plasmaspheric hiss. Their model produced high-energy proton enhancement as a result of energy diffusion. The diffusion timescale is on the order of tens of days, which seems to be long but it is comparable to charge exchange and Coulomb loss lifetimes of H^+ at these energies. Once again, we have demonstrated the roles of whistler mode waves in ionosphere-plasmasphere-ring-current-radiation-belt coupling: the ionosphere and plasmasphere provide the environment for whistler mode wave generation and excitation; in turn, these waves cause precipitation of the radiation belt electrons and energization of the ring current ions.

2.3. Magnetic depression produced by the ring current

The magnetic field disturbances generated by the ring current produce noticeable signatures on both ground-based and satellite magnetometers. In fact, the magnetic disturbances measured on ground are used to define a magnetic storm as indicated by the Dst (disturbance, storm-time) index (Daglis, 2003). During extreme active periods, the magnetic depression produced by the ring current on the surface of the Earth reaches a maximum of 300–600 nT, which is about 1–2% of the main field. In the magnetosphere, the relative importance of the ring current field is much higher. Using magnetometer data from several satellites during storm-times ($Dst \leq -65$ nT), Tsyganenko *et al.* (2003) found strong distortion of the magnetic field in the inner magnetosphere. The disturbed field reaches 30–50% of the main field at 3 earth radii (R_E) at the equator during major storms.

The drift paths of charged particles in the magnetosphere are altered by the distorted magnetic field, especially for radiation belt particles, for which magnetic drifts are dominant over electric drifts. To demonstrate this effect, Fig. 5 plots the drift paths of energetic electrons with magnetic moment 1.2×10^{10} keV/T and pitch angle 90°, which have been significantly distorted by the ring current field perturbations. The magnetic field is modeled by the Tsyganenko 1996 (T96) model (Tsyganenko, 1995). Input parameters for T96: solar wind dynamic pressure, interplanetary magnetic field (IMF) By and Bz are set to be 3 nPa, 0 nT and -5 nT, respectively. The Dst index, which is also an input parameter of the T96 model, is set to be 0 nT (left panel) and -80 nT (right panel) to represent weak and strong disturbances from the ring current. In Fig. 5, drift paths (solid lines) are calculated including corotation and convection, which is assumed to be Volland-Stern type (Volland, 1973; Stern, 1975) with cross polar cap potential drop of 60 kV. Dashed lines indicate the energy of the electrons. As shown in the left panel, electrons with this particular magnetic moment, at 5.5 R_E, 00 MLT, have energy of 1.5 MeV and travel in closed drift paths. However, in the

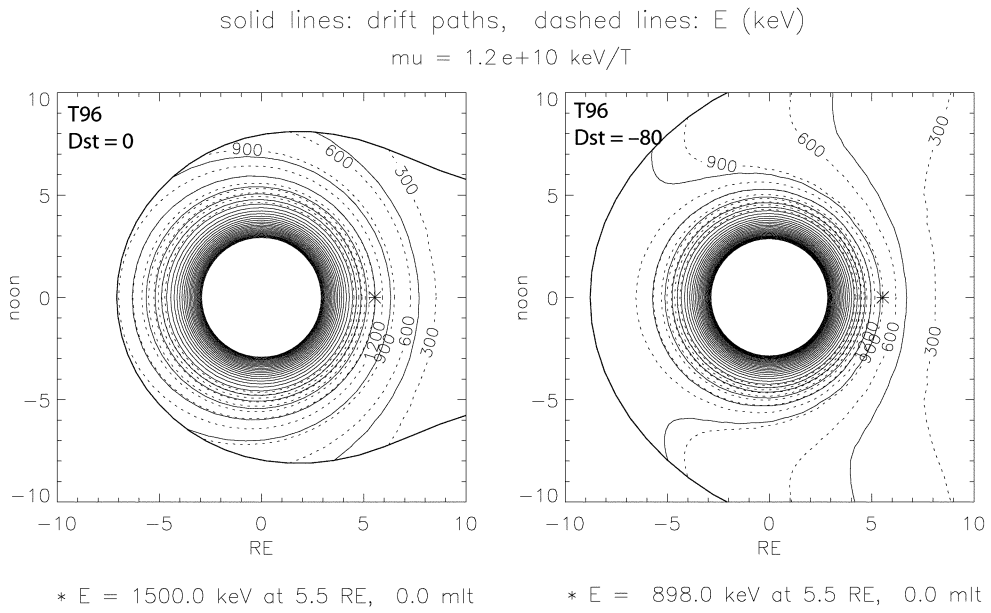

Fig. 5. Drift paths of equatorially mirroring electrons with magnetic moment equal 1.2×10^{10} keV/T. Left panel shows the drift paths (solid lines) and energy contours (dashed lines) in T96 model with input parameters: solar wind dynamic pressure=3 nPa, Dst=0, IMF By=0, and Bz=−5 nT. The right panel is the same as the left one except Dst in T96 model is equal to −80 nT.

magnetosphere that is inflated by the ring current (right panel), the same particles (same all three adiabatic invariants) cross midnight at a distance greater than $5.5\,R_E$ in open drift path, with a much lower energy (<900 keV). This calculation illustrates the effect of the ring current on radiation belt dynamics through the magnetic field produced by the ring current.

It is well-observed that radiation belt electron fluxes decrease during storm main phases and then gradually increase toward pre-storm level during recovery. As discussed in the Introduction, the flux dropout during storm intensification is an adiabatic effect as radiation belt particles are drifting in a field strongly distorted by the ring current. However, both studies from Kim and Chan (1997) and Reeves *et al.* (2003) indicated that the fully adiabatic effect accounts for a significant fraction not all of observed flux variations. Other loss and source mechanisms have to be involved. In order to separate influences from adiabatic and non-adiabatic processes, ring current-generated field has to be considered in analytical or simulation studies of the radiation belt. Zheng *et al.* (2003) included the Dst effect in their radiation belt environment model by simply employing the T96 model with Dst as one of the parameters. They were able to reproduce the flux dropout observed during the main phase of the storm on 12 August 2000. On the other hand, a number of models and studies take into account the ring current effects in a self-consistent manner. Modelers at the University of Michigan have coupled the Block-Adaptive-Tree-Solarwind-Roe-Upwind-Scheme (BATSRUS) MHD with the Rice Convection Model (RCM) such that particle pressure

generated by the ring current is included in the MHD equation to calculate the global magnetospheric fields (Gombosi *et al*., 2003; De Zeeuw *et al*., 2004). They found the coupled code produces significant higher pressure and much more inflated magnetic field in the inner magnetosphere than the MHD model alone. Another technique to achieve self-consistency of particles and fields is the force equilibrium approach, which considers the balance between pressure gradient and magnetic stress ($J \times B = \nabla p$). Lemon *et al.* (2004) simulated plasma transport from the plasma sheet to the ring current using the coupled code of the RCM and the Magneto-Friction (MF) code (Toffoletto *et al*., 2001). Particle pressure calculated by the RCM is passed to and overrides the pressure in the MF code. The MF code then computes a new equilibrium magnetic field that satisfies the force balance condition. The new magnetic field is passed back to the RCM to complete the computation cycle. With this self-consistent model, Lemon *et al.* (2004) found that the perturbation associated with the injection of plasma sheet ions in the inner magnetosphere prevents the formation of a significant ring current, unless there is a substantial reduction of the specific entropy $PV^{5/3}$ in inner plasma sheet. Here, P is particle pressure and V is flux volume per unit magnetic flux.

3. Magnetosphere-ionosphere coupling

3.1. Magnetospheric sources of ionosphere heating

As discussed in detail in the last section, the plasmasphere is heated by the ring current plasmas through Coulomb and wave-particle interactions. The interesting remaining question is whether the ring current energy deposited in the plasmasphere is transported down to the ionosphere and produce observable signatures there. One possible transport mechanism is heat conduction along magnetic field lines. In a fully ionized gas, the plasma is considered as collisional and conduction is effective when the mean free path of self-collision (Coulomb) is less than the particle scale height. Cole (1965) estimated the electron mean free path and scale height along a flux tube of $L = 2.5$, assuming an equatorial plasmaspheric density n_e of $10^3\,\mathrm{cm}^{-3}$ and $n_e \propto B$. He found heat conduction at the equator is poorly justified but is acceptable at higher latitudes ($\lambda > 25^\circ$) where thermal density is higher. It thus requires a flux of electrons to carry the heat energy out of the equator. Bounce motion is the ideal process to bring the heated electrons from the equator to the collisional region of higher latitudes. As a result, the criterion for heat conduction is instead determined by the relative collision time to the bounce period. If the collision time t_c is shorter than the bounce period t_b, the plasma is considered to be collisional. The Coulomb electron-electron collision time is $t_c \sim 1.6 \times 10^4 n_e^{-1} T_e^{3/2}$ (Spitzer, 1962) where t_c is in seconds, n_e is density in cm^{-3} and T_e is electron temperature in eV. At $L = 3$, $t_b \sim 1.2 \times 10^2 T_e^{-1/2}$. For a typical plasmasphere of $T_e = 1$ eV and $n_e = 1000\,\mathrm{cm}^{-3}$, t_c is less than t_b and the plasmaspheric electrons are collisional.

Cornwall *et al.* (1971) proposed that the ring current energy dissipation to the plasmasphere electrons via Coulomb and wave-particle interactions, conducts along the flux tube as a heat flux to the ionosphere. This magnetospheric influx heats the ionospheric electrons and produces the subauroral T_e peak and the associated optical signature named by stable auroral red (SAR) arc which is often observed during the recovery of magnetic storm (Fig. 1). The subauroral T_e peak is an enhancement in the

latitudinal profile of electron temperature in the subauroral *F* region (Brace *et al*., 1967, 1974; Kozyra *et al*., 1986; Fok *et al*., 1991b). The peak values are typically in excess of ~3000 K and the latitudinal extent is ~2–3°. SAR arc is formed at the location of electron temperature enhancements. It is narrow in latitude but extends in longitude around the nightside and even possibly to the dayside. When the electron temperature is high and above 3000 K, significant amount of electrons with energies in excess of 1.96 eV exist in the high-energy tail of the Maxwellian distribution. These electrons collisionally excite O atoms to the ^1D state. The excited O atoms radiatively relax with the emission of photons at 6300 or 6364 Å. SAR arc emission rate ranges from barely above the airglow level to several kilorayleighs (Rees and Roble, 1975). Simulation studies performed by Kozyra *et al.* (1987) and Fok *et al.* (1993) suggested that Coulomb collisions alone are sufficient to extract energy from the storm-time ring current, mainly from ring current O^+, to the cold plasmasphere to generate the SAR arc emissions to the observable levels. The role of wave-particle interactions is still unclear.

The Coulomb proton-proton collision time is 43 times of that of the electrons because the collision time is proportional to the square root of the atomic mass. Ions trapped in the plasmasphere could be considered as collisionless. Comfort *et al.* (1995) calculated the ion conductivity in the plasmasphere considering contribution only from ions that lie inside the loss cone. Using this reduced ion conductivity in their hydrodynamic model, they were able to reproduce the high ion temperatures (1–2 eV) observed in the outer plasmasphere and obtained substantially lower ion temperatures in the topside ionosphere. Since the ion conductivity is low, thermal energy from the heated plasmaspheric ions may hardly conduct to the ionosphere to cause enhanced ion temperature there. Ion temperature within the SAR arc has been measured but in one case enhancement was found but in another case no enhancement at all (Rees and Roble, 1975). Therefore it is still not clear how much of the ring current energy deposited in plasmaspheric ions is transported down to the ionosphere and lost there.

3.2. Ionosphere as a source of magnetospheric ions

The ionospheric source consists of a highly variable flow of heavy ions superposed upon a relatively steady flow of hydrogen (and to a lesser extent, helium) ions. The local H^+ flux may exceed $1\times10^{12}\,m^{-2}s^{-1}$ (Moore *et al*., 1999) when "normalized" to 1000 km altitude using a dipolar magnetic flux tube area profile. The H^+ source is weakly dependent on solar EUV radiation and therefore on solar cycle phase, with lower fluxes at solar maximum. This results from reductions in H density in the altitude range where free H^+ is produced by charge exchange of O^+ produced by solar photoionization. The outer flux tubes of the magnetosphere circulate on paths linking the boundary layers, and exhaust plasma to the solar wind faster than it is refilled from the ionosphere. These polar flux tubes are perpetually in a state of disequilibrium with a steadily flowing light ion polar wind (Moore *et al*., 1999).

Somewhat deeper in the magnetosphere, where flux tube circulation occasionally links to the boundary layers (Goldstein *et al*., 2002), a slower form of the polar wind is known as "refilling flows". In the innermost magnetosphere, the plasmasphere, closed circulation traps outflowing plasma and accumulates it to pressure equilibrium, effectively shutting down the outflow. The plasmasphere is severely depleted in O^+ and other

heavy ions, relative to the ionosphere. Varying solar illumination modulates electron densities and temperatures, producing a diurnal "breathing" of the plasmasphere. But heavy ion scale heights remain much smaller than the height of the closed region, so these ions remain confined by gravity to relatively low altitudes.

The variable component of plasma outflow consists principally of escaping oxygen ions (O^+), typically with ~10% N^+, which we term the auroral wind. Highly variable amounts of the molecular species N_2^+, NO^+, and O_2^+ escape with the O^+, but these fluxes are important mainly for the largest solar wind disturbances. The total heavy ion flux varies in space and time from essentially zero to greater than $1 \times 10^9\,cm^{-2}s^{-1}$ (at the standard altitude of 1000 km). Appreciable heavy ion outflow fluxes are found only in the auroral zones or within polar cap auroral features where electrons or ions are heated and heavy ion scale heights increase substantially. Such flows respond directly to the deposition of solar wind energy in the topside ionosphere (Strangeway *et al*., 2000). The dayside auroral zone, or cusp "footprint" is the most productive region of auroral wind, and the most directly responsive to solar wind conditions (Moore *et al*., 1999). Figure 6 illustrates the gross dependence of auroral wind outflows on solar wind dynamic pressure fluctuations, which appear to play a significant role in delivering energy to the ionosphere.

The sources of heavy ion plasma outflows are localized and depend strongly on solar wind conditions, but the resulting outflows circulate throughout the magnetosphere on high latitude flux tubes that participate in all aspects of magnetospheric dynamics. The large outflows from the dayside auroral zone are circulated antisunward across the polar cap, forming a fountain of plasma that is strongly influenced by both gravity and solar wind electromagnetism. In particular, the cooler component

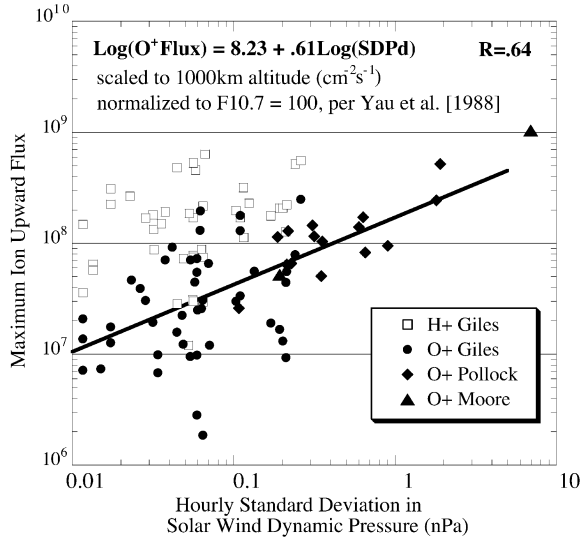

Fig. 6. The observed relationship between ionospheric auroral wind fluxes and the hourly average standard deviation of the solar wind dynamic pressure. Here the long term solar cycle of F10.7 has been removed according to the scaling of Yau and Lockwood (1988).

of the plasma launched upward in the dayside cusp region falls back into the polar ionosphere, while the hotter, faster component continues along lobe field lines to the magnetotail. Thus we typically have simultaneous outflow at high altitude and downflow at lower altitudes on polar cap/lobe field lines (Chandler, 1995). As the fountain of heavy-ion plasma expands along each flux tube, both inward and outward, the high altitude O^+ density drops.

Polar ionospheric outflows are channeled directly into the night side plasma sheet. The strong dynamics of this region are known to contribute to the formation of storm time plasmas in the inner magnetosphere. However, both simple calculations (Hill, 1974) and elaborate simulations (Moore *et al*., 2005a) agree on the conclusion that the polar wind H^+ pressure in the inner magnetosphere is for typical conditions overwhelmed by the pressure of solar wind protons entering into the magnetosphere, mostly through the flank magnetopause. However, polar wind protons are sufficiently plentiful to produce densities comparable with the density of solar wind ions finding their way into the inner magnetosphere. However, they are not typically heated or energized sufficiently to become a competitive pressure contribution. Observations (Hamilton *et al*., 1988) and recent simulations (Moore *et al*., 2005b) agree on the conclusion that the auroral wind produces substantial pressure in the inner magnetosphere and competes with the solar wind proton pressure contribution. This requires both strong energy dissipation in the auroral zone ionosphere and strong circulation flows in the magnetosphere as a whole.

3.3. Electric coupling between magnetosphere and ionosphere

3.3.1. Field aligned currents

The magnetosphere and ionosphere are tightly connected through magnetic field lines and the current flow along them. The divergence of gradient-curvature drift currents generated by plasmas in the magnetosphere, mainly from ring current ions, produces field-aligned currents that flow into or out from the ionosphere. These currents must close through the ionosphere. The thickness of the ionospheric current layer is relatively small in comparison with that in the magnetosphere. In the thin-layer assumption, the continuity of current satisfies the equation:

$$\nabla \cdot (-\Sigma \cdot \nabla \Phi_i) = J_{\parallel} \sin I, \tag{1}$$

where Σ is the height-integrated conductivity tensor, Φ_i is the electric potential and I is the inclination of the geomagnetic field. The ring current acts as a current generator. For given Σ and $J_{\parallel}$, the electric potential distribution in the ionosphere is obtained by solving (1). The above formulation is valid if temporal changes in the driver (perpendicular current in the magnetosphere for this particular case) are much longer than the Alfvén wave propagation time between the magnetosphere and the ionosphere. Information in the magnetospheric usually takes a few minutes to propagate in the form of Alfvén wave from the equatorial plane to the ionosphere (Baumjohann and Glaßmeier, 1984).

The field-aligned currents generated by the ring current modulate the ionospheric electric potential and plasma flow distribution. The newly restructured electric potential is mapped to the magnetosphere along field lines, placing a load on the magneto-

spheric electric generator, which is powered by plasma convection. The motion of magnetospheric particles is thus significantly influenced by this self-consistently coupled system (Vasyliunas, 1970; Wolf, 1970).

3.3.2. Shielding electric field

Non-uniformity in the plasma pressure in the inner magnetosphere produces the Region 2 field-aligned current generally flowing into the ionosphere on the duskside and away from the ionosphere on the dawnside. The Region 2 field-aligned current thus produces an ionospheric electric field that is opposite to the dawn-to-dusk convection electric field. This additional electric field shields or partially shields the inner region of the magnetosphere from the convection electric field. For this reason, the additional electric field is called the shielding electric field. When the dawn-to-dusk convection field is suddenly weakened while the Region 2 field-aligned current remains fairly constant, the shielding electric field may dominate over the convection field and overshield the region earthward of the Region 2 field-aligned current (Spiro *et al*., 1988; Peymirat *et al*., 2000). Simulation results from the RCM have shown that overshielding takes place when the IMF turns northward after a prolonged southward IMF condition, and the lifetime of the overshielding condition lasts for about 10–20 min (Spiro *et al*., 1988). This prediction is consistent with observations of the ionospheric electric field at the MillStone Hill, Chatanika, and Jicamarca radars reported by Kelley *et al.* (1979) and Fejer *et al.* (1990).

Ebihara *et al.* (2004) calculated the ionospheric potential pattern using the Comprehensive Ring Current Model (CRCM) (Fok *et al*., 2001), with the aurora-associated conductivity based on the IMAGE/FUV observation. They found that the overshielding condition is established when the auroral conductivity rapidly decreases after a prolonged southward IMF condition. When the conductivity reduces abruptly, the shielding electric field becomes strong. A dusk-to-dawn electric field (or the antisunward plasma flow) is expected to exist in the region where the aurora-associated conductivity is lower than ambient. Overshielding also happens during northward turning of the IMF. Goldstein *et al.* (2002) performed simulations by the Magnetospheric Specification Model (Freeman *et al*., 1993) and produced dusk-to-dawn overshielding electric field triggered by sudden, strong northward turning of the IMF. They found the antisunward flow caused by overshielding creates a shoulder-shaped bulge in the morning sector plasmapause, named as the plasmaspheric shoulder (Burch *et al*., 2001).

The shielding effect tends to impede the plasma injection from the plasma sheet. When the magnetosphere is not coupled with the ionosphere, doubling the plasma sheet density simply doubles the ring current strength (*e.g*., Chen *et al*., 1994; Kozyra *et al*., 1998; Jordanova *et al*., 1998). However, the degree of the shielding increases with increasing the plasma sheet density (Garner, 2003). When the magnetosphere is electrically coupled with the ionosphere, doubling the plasma sheet density does not double the ring current strength because of the increasing shielding field. The CRCM simulation showed that the ring current total energy is roughly proportional to $N_{ps}^{1/2}$, where N_{ps} is the plasma sheet density (Ebihara *et al*., 2005). This non-linear response comes from the intense shielding electric field for dense plasma sheet.

The drift trajectories of magnetospheric ions are drastically skewed by the shielding

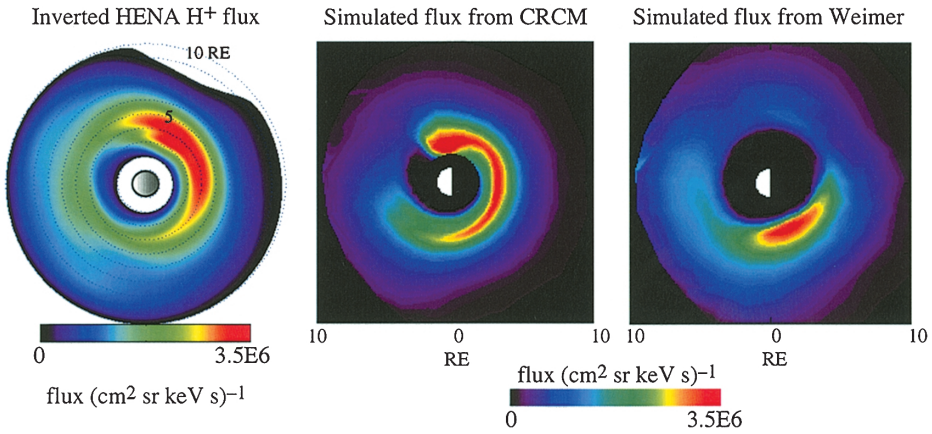

Fig. 7. Left panel: equatorial flux of 27–39 keV H^+ inverted from the HENA image at 0900 UT on 12 August 2000. Middle panel: simulated flux at the same energy range and time calculated by the CRCM. Right panel: simulated flux using the Weimer electric field model. Sun is to the left in all panels. Note that the colors of the HENA flux and that of the simulated fluxes are slightly different.

electric field. Conventionally, the tens-of-keV ions originating from the nightside plasma sheet are thought to reach a minimum L-value in the pre-midnight region as predicted by drift calculation using statistical electric field models (*e.g.*, Stern, 1973; Volland, 975; Weimer, 2001). However, during major storms when shielding electric field is strong, the CRCM predicted that the tens-of-keV ions originating from the nightside plasmas sheet reaches a minimum L-value in the post-midnight region instead (Fok *et al.*, 2003; Ebihara and Fok, 2004). Fok *et al.* (2003) have shown that, for the same storm condition, calculations with Weimer type convection electric field produced peak ion flux in the pre-midnight sector, while the self-consistent model of the CRCM predicted the peak in the post-midnight sector. Figure 7 shows the equatorial flux of 27–39 keV H^+ inverted from the HENA image (Perez *et al.*, 2001) at 0900 UT on 12 August 2000 (left panel), showing a flux maximum near dawn. The middle panel plots the simulated flux at the same energy range and time calculated by the CRCM. As shown in the figure, the CRCM produces a comparable flux level and a similar local-time distribution as the HENA invert ion flux. In contrast, the simulation using the empirical electric field model of Weimer (1995) gives the peak flux at the dusk-midnight sector (right panel). The post-midnight enhancements of ring current ion fluxes with energy of tens of keV are consistent with ENA observations by the IMAGE/HENA during over 10 storms in 2000–2002 (Brandt *et al.*, 2002). The strong shielding electric field established in the inner magnetosphere is believed to be the main contributor of this newly found feature (Ebihara and Fok, 2004).

3.3.3. Subauroral polarization stream

In the dusk-to-midnight region during geomagnetic active times, very often there is a rapid westward flow in the ionosphere just equatorward of the auroral oval, called the Polarization Jet (PJ) (Galperin *et al.*, 1974) or the SubAuroral Ion Drift (SAID)

(Spiro *et al*., 1978). The SAID is latitudinally confined, and usually, it is about 1 degree wide in latitude. The flow speed often exceeds 2.5 km/s (Spiro *et al*., 1978). The SAID is associated with a spike of an intense poleward electric field observed in the subauroral region (Smiddy *et al*., 1977; Maynard; 1978). The associated poleward electric field ranges up to over 400 mV/m and the potential across these structures is approximated to lie between 1 and 10 kV at 600–1750 km altitudes, according to Freja observations (Karlsson *et al*., 1998). Statistical studies demonstrate that most of the SAID occurs in between 1800 and 0200 MLT and between 55 deg and 70 deg invariant latitude (Spiro *et al*., 1979; Karlsson *et al*., 1998). Approximately 85% of the SAID are observed in association with well-defined *F*-region troughs. However, only about 20% of mid-latitude troughs observed by AE-C are accompanied by SAID (Spiro *et al*., 1979). The SAID is also observed in association with downward field-aligned currents. Rich *et al.* (1980) observed net downward field-aligned currents of the order of 1 A/m^2 in the region of strong subauroral electric fields ranging up to 350 mV/m. The close connection with the net downward field-aligned current supports the following scenario for the formation of SAID: the field-aligned currents flow into the subauroral ionosphere and close through the low-conductivity region equatorward of the auroral oval, producing a strong poleward directed electric field (Southwood and Wolf, 1978; Banks and Yasuhara, 1978; Anderson *et al*., 1993).

Recently, based on observations of the MillStone Hill radar, Foster and Burke (2002) introduced the name SubAuroral Polarization Stream (SAPS) to encompass both types of observed subauroral electric fields, the SAID/PJ signatures and the similar feature in broader regions described by Yeh *et al.* (1991). The SAPS structure has an average peak amplitude of 900 m/s or higher and spans 3–5 degrees in latitude (Foster and Vo, 2002). Foster and Vo (2002) suggested that SAPS is associated with magnetosphere-ionosphere (M-I) coupling and is caused by field-aligned current trying to close across the subauroral ionosphere, as same as the proposed formation mechanism for the SAID.

It has been observed that rapid westward flow also exists in the magnetosphere (Maynard *et al*., 1980; Rowland and Wygant, 1998), appeared to be associated with the SAPS. Rowland and Wygant (1998) carried out a statistical study of the dawn-to-dusk electric field observed by the Combined Radiation and Release Satellite (CRRES) near the equatorial plane. The averaged dawn-to-dusk electric field shows that for low *Kp* values (between 0 and 3), the magnitude of the electric field increases with *L*. This is consistent with a simple convection electric field model with a shielding effect (Stern, 1975; Volland, 1978). However, for moderate *Kp* values (between 4 and 7^-), the magnitude of the dawn-to-dusk electric field has a local peak near $L = 3$–4. Then when *Kp* ranges between 7 and 9, the magnitude decreases with *L*. These *in-situ* measurements in the magnetosphere illustrate that simple Volland-Stern type model cannot represent disturbed conditions. The actual convection electric field is far more complicated by processes coupling the magnetosphere and ionosphere, such as the shielding field and the SAPS.

3.4. Roles of ionospheric conductivities in M-I coupling

The ionospheric conductivity plays an active role in the M-I coupling. Equation

(1) illustrates that for a given field-aligned current, the magnitude of the electric field (potential gradient) decreases with increasing the conductivity. This implies that the magnitude of the shielding electric field and the SAPS electric field will be weakened when conductivity is high. Spiro and Wolf (1984) found that the total energy of the ring current increases by a factor of 1.4 when the ionospheric conductivity is doubled. Using the CRCM, Ebihara *et al.* (2004) investigated how the ionospheric conductivity influences the ring current development. They found the conductivity for F10.7$=250\times10^4$ Jy (solar maximum condition) results in the ring current that is about 29% stronger than for that for F10.7$=70\times10^4$ Jy (solar minimum condition). The conductivity at equinox results in the ring current that is about 5% stronger than at solstice. The ionospheric conductivity in the subauroral region is the higher at the solar maximum and equinox, therefore the magnitude of the shielding electric field is weaker. During these time periods, the plasma originating from the plasma sheet drifts further earthward by the convection electric field because the inner magnetosphere is less shielded. As a consequence, a more robust ring current is developed.

The relative latitude of the auroral oval also influences the ring current formation. Both expansion and contraction of the auroral oval from an optimal latitude is found through simulation to weaken the ring current strength (Ebihara *et al*., 2004). Mesoscale structures in the conductivity associated with auroral precipitation are shown to result in a significant modification of the electric field distribution and the plasma distribution as mentioned in the previous section. When the auroral conductivity decreases, the overshielding condition is produced, causing the anti-sunward plasma flow in the magnetosphere.

The already low conductivity in the SAPS region is further reduced by the increased frictional heating of the ionospheric ions. The frictional heating increases the rate of ion-atom interchange between O^+ and N_2. Subsequent fast recombination of NO^+ with electrons further reduces the subauroral *F* region conductivity. The heating also leads to a thermal expansion, substantial field-aligned plasma flow and large depression in the concentration in the *F* region, known as the mid-latitude trough. When the ionospheric concentration is reduced, the conductivity is decreased and then speed of the SAPS is increased. Fast SAPS increases the frictional heating, in turn resulting in the reduction of the conductivity. This self-enhanced mechanism has been proposed by Anderson *et al.* (1993). The ring current thus tightly links with not only the ionosphere but also the thermosphere.

4. Discussions and summary

We have illustrated the close connections between plasma populations in the inner magnetosphere and the ionosphere. Even though numerous observation and simulation studies have been carried out to tackle this subject, the linkage is so extensive and complex that there are still missing pieces in understanding the overall picture of these coupled systems. The impact of wave-particle interactions is one of the major unresolved questions. Ring current precipitation loss due to interactions with EMIC waves is often thought to be important and should not be ignored (Kozyra *et al*., 1997a; Jordanova *et al*., 2001). However, it is not clear how this process contributes to the

ring current loss and especially, the rapid decay of the ring current often seen during early recovery. Kozyra *et al.* (1997a) included EMIC wave scattering in their ring current simulation and found just an additional ~8 nT recovery of the Dst index at the early recovery phase of a storm with minimum Dst of −150 nT. Moreover, EMIC waves are rarely observed in the magnetosphere at $L < 5$ (Anderson *et al*., 1992), where the peak of the ring current located during the main and early recovery phases. The relative roles of EMIC waves and Coulomb interaction in heating the plasmasphere are still controversial. Simulations including either one of the two mechanisms alone provide sufficient heating to the plasmasphere and produce observable high temperatures there (Gorbachev *et al*., 1992; Fok *et al*., 1993, 1995).

SAR arcs provide an excellent display of energy transport from the ring current to the magnetically connected underlying ionosphere. Observations reveal significant amounts of O^+ (major source of plasmaspheric electron Coulomb heating) in the storm time ring current (Hamilton *et al*., 1988; Daglis *et al*., 1993). The lack of EMIC waves in the SAR energy source region (Anderson *et al*., 1992), implicates Coulomb collision as a favorable energy exchange process over wave-particle interaction. However, this deduction is not yet decisive (Kozyra *et al*., 1997b). Another puzzle in SAR arc physics is the co-existence of a soft (~1 eV) electron precipitation over SAR arcs (Gurgiolo *et al*., 1982; Slater *et al*., 1987). Any SAR arc energy source theory should provide the explanation of this electron precipitation. Even though Coulomb collision mechanism is very convincing, it is not certain whether Coulomb collisions alone will produce such field-aligned soft electron distribution.

As we have discussed above, magnetospheric O^+ is a one of the key players in the coupling processes in the M-I system. Auroral O^+ outflow provides substantial pressure in the ring current comparable with the solar wind protons (Moore *et al*., 2005b). O^+ is the dominant source of plasmaspheric electron heating (Kozyra *et al*., 1987). In fact, O^+ in the ring current would suppress the growth of EMIC waves and lower the frequency of maximum wave growth (Kozyra *et al*., 1984). Recent observations from IMAGE/HENA revealed important but relatively short-lived enhancements of 52–180 keV O^+ at substorm expansions (Mitchell *et al*., 2003). It is not certain that how these heavy ions get energized and injected into the ring current region. It may be through direct injection from the ionosphere or energization of the pre-existing lower-energy ions. Further observational and simulation investigations are needed to understand the transport and energization of the O^+ ions and their influences in coupled M-I system.

We have demonstrated the effects of ring current-generated magnetic distortion on radiation belt development. Work has been done to include the ring current field in global modeling (De Zeeuw *et al*., 2004; Lemon *et al*., 2004). However, none of them has incorporated the self-consistent fields into radiation belt calculation.

In recent years, the space physics community has recognized the need for multi-point measurements and global imaging to monitor the coupling and simultaneous responses of various plasma populations in the magnetosphere and ionosphere to solar activity and to the resultant disturbances in the interplanetary medium. The IMAGE mission, launched on 25 March 2000, is the first mission dedicated to imaging the aurora, ring current, plasmasphere and ionosphere outflow (Burch, 2000). Later in the same year, the 4 satellites of the Cluster II missions were launched, carrying plasma

instruments to measure electric and magnetic fields, electron and ion distributions. This tetrahedral constellation was designed to study the small-scale plasma structures and macroscopic turbulence in three-dimensions in the regions of the solar wind, bow shock, magnetopause, cusps, auroral zone and the magnetotail (Escoubet *et al*., 2001). The complementary capabilities of these two missions have enabled many unique observations and scientific discoveries (http://image.gsfc.nasa.gov/poetry/IMAGEdisc.html/, http://sci.esa.int/cluster/). At least three multi-point and global imaging missions are being implemented and scheduled to launch in the next 10 years: TWINS (Two Wide-angle Imaging Neutral-atom Spectrometers), THEMIS (Time History of Events and Macroscale Interactions during Substorms), and MMS (Magnetospheric MultiScale Mission).

In parallel on the theory-modeling side, end-to-end global models have been developed that transmit the disturbances on the surface of the Sun through the interplanetary space to the Earth's magnetosphere, ionosphere and lastly, the atmosphere. These modeling activities have been vigorously pursued in several modeling centers such as the Center for Space Environment Modeling at the University of Michigan, the Community Coordinated Modeling Center at the Goddard Space Flight Center, and the Center for Integrated Space Weather Modeling at NSF. Measurements from current and future imaging and multi-point missions are vital for testing the theories and refining the models. On the other hand, theories and models would be used to guide the interpretations of observational data and to provide assistance in future mission designs. Combining the efforts and strengths of global missions and large-scale modeling, we foresee major breakthroughs will be made in unveiling the physics that governs the interactions in the entire M-I system and their responses to the solar wind.

We have reported results from investigations on coupling between plasmas in the inner magnetosphere and their connection with the ionosphere:

(1) Significant energy is transferred from ring current ions to the plasmasphere through Coulomb collisions and produces observable plasmaspheric electron and ion temperature enhancements.

(2) Anisotropies in ring current particle distributions provide the free energy for plasma wave excitation. EMIC waves, whistler mode chorus and plasmaspheric hiss are commonly observed in the inner magnetosphere. These waves cause pitch-angle and energy diffusion of the ring current and radiation belt plasmas. The damping of these waves in the plasmasphere is a source of plasmaspheric heating.

(3) The magnetic field generated by the ring current during storm intensification modifies the main field in the inner magnetosphere and alters the drift paths of radiation belt particles, causing reversible adiabatic decrease and irreversible loss in radiation belt flux.

(4) Energy from the high-temperature plasmaspheric electrons is transported along field lines to the ionosphere and produces the observed electron temperature enhancements in the subauroral *F*-region during magnetic storms. These electron temperature enhancements are energy sources for the SAR arc emissions at mid-latitude ionosphere.

(5) The auroral zone is the vital source of the heavy ion pressure seen in the magnetosphere and this source is highly modulated by the fluctuations in the solar wind dynamic pressure as reflected in local auroral conditions. The ionosphere also provides proton

density in the magnetosphere comparable to the solar wind source.
(6) The magnetosphere and the ionosphere are tightly linked together through magnetic field lines and the field-aligned currents.
(7) The shielding electric field is a result of electric coupling between the magnetosphere and ionosphere. The non-linear response of the ring current to the plasma-sheet source and several newly observed features in the inner magnetosphere, such as plasmasphere shoulder, post-midnight enhancement in storm-time ring current flux, are effectively explained by the shielding effect.
(8) SAPS and SAID are typical signatures of M-I coupling, caused by field-aligned current trying to close across the low-conductivity region in the subauroral ionosphere.
(9) Ionospheric conductivities play a crucial role in determining the convection electric fields in the ionosphere and the inner magnetosphere, and thus the transport and development of the ring current.

We have identified the following unanswered issues in inner-magnetosphere-ionosphere interactions that need further investigation.
(1) The precise roles of EMIC waves in ring current decay.
(2) The relative importance of plasma waves and Coulomb collisions in plasmasphere heating.
(3) The exact cause of the ring current rapid decay at the early recovery phase.
(4) The source of the soft-electron precipitation associated with the SAR arcs.
(5) The sources of the instant O^+ enhancement in response to substorm expansion.
(6) The relative roles of wave induced energy-diffusion versus earthward radial diffusion in producing the radiation belt electron enhancements often seen in the recovery phases of magnetic storms.

The above unresolved questions can be addressed through the careful cross analysis of observations from the ongoing and future imaging and multi-point missions with simulation results of large-scale modeling.

Acknowledgments

We thank Drs. Janet Kozyra, Pontus Brandt, Adolfo Vinas, Robert Benson, George Khazanov, Dimitris Vassiliadis, Richard Wolf, and Vania Jordanova for useful discussions. The HENA inverted H^+ flux shown in Fig. 7 is provided by Dr. Joseph Perez. This work is supported by the NASA Office of Space Science Sun-Earth Connection Guest Investigator Program under RTOP Grant 370-16-00-11 and IMAGE mission under UPN 370-28-12.

The editor thanks Dr. J. Burch and another referee for their help in evaluating this paper.

References

Albert, J.M. (1994): Quasi-linear pitch angle diffusion coefficients: Retaining high harmonics. J. Geophys. Res., **99**, 23741–23745.

Anderson, P.C., Heelis, R.A. and Hanson, W.B. (1991): The ionospheric signatures of rapid subauroral ion drift. J. Geophys. Res., **96**, 5785–5792.

Anderson, B.J., Erlandson, R.E. and Zanetti, L.J. (1992): A statistical study of Pc 1–2 magnetic pulsations in the equatorial magnetosphere, 1. Equatorial occurrence distributions. J. Geophys. Res., **97**, 3075–3088.

Anderson, P.C., Hanson, W.B., Heelis, R.A., Craven, J.D., Baker, D.N. and Frank, L.A. (1993): A proposed production model of rapid subauroral ion drifts and their relationship to substorm evolution. J. Geophys. Res., **98**, 6069–6078.

Baker, D.N., Kanekal, S.G., Looper, M.D., Blake, J.B. and Mewaldt, R.A. (1996): Jovian, Solar, and other possible sources of radiation belt particles. Radiation Belts: Models and Standards, ed. by J.F. Lemaire *et al.* Washington, D.C., Am. Geophys. Union, 49–55 (Geophysical Monograph Vol. 97).

Banks, P.M. and Yasuhara, F. (1978): Electric fields and conductivity in the nighttime E region: A new magnetosphere-ionosphere-atmosphere coupling effect. Geophys. Res. Lett., **5**, 1047–1050.

Baumjohann, W. and Glaßmeier, K.H. (1984): The transient response mechanism and Pi 2 pulsations at substorm onset-review and outlook. Planet. Space Sci., **32**, 1361–1370.

Blake, J.B., Kolasinski, W.A., Fillius, R.W. and Mullen, E.G. (1992): Injection of electrons and protons with energies of tens of MeV into $L < 3$ on 24 March 1991. Geophys. Res. Lett., **19**, 821–824.

Brace, L.H., Reddy, B.M. and Mayr, H.G. (1967): Global behavior of the ionosphere at 1000-kilometer altitude. J. Geophys. Res., **72**, 265–283.

Brace, L.H., Maier, E.J., Hoffman, J.H., Whitteker, J. and Shepherd, G.G. (1974): Deformation of the night side plasmasphere and ionosphere during the August 1972 geomagnetic storm. J. Geophys. Res., **79**, 5211–5218.

Brandt, P.C., Ohtani, S., Mitchell, D.G., Fok, M.-C., Roelof, E.C. and Demajistre, R. (2002): Global ENA observations of the storm mainphase ring current: Implications for skewed electric fields in the inner magnetosphere. Geophys. Res. Lett., **29** (20), 1954, doi: 10.1029/2002GL015160.

Braysy, T., Mursula, K. and Marklund, G. (1998): Ion cyclotron waves during a great magnetic storm observed by Freja double-probe electric field instrument. J. Geophys. Res., **103**, 4145–4155.

Burch, J.L. (2000): IMAGE mission overview. Space Sci. Rev., **91**, 1–14.

Burch, J.L., Mitchell, D.G., Sandel, B.R., Brandt, P.C. and Wuest, M. (2001): Global dynamics of the plasmasphere and ring current during magnetic storms. Geophys. Res. Lett., **28**, 1159–1162.

Carpenter, D.L. (1963): Whistler evidence of a 'knee' in the magnetospheric ionization density profile. J. Geophys. Res., **68**, 1675–1682.

Chandler, M.O. (1995): Observations of downward moving O^+ in the polar topside ionosphere. J. Geophys. Res., **100**, 5795–5800.

Chen, M.W., Lyons, L.R. and Schulz, M. (1994): Simulations of phase space distributions of storm time proton ring current. J. Geophys. Res., **99**, 5745–5760.

Chua, D., Brittnacher, M., Parks, G., Germany, G. and Spann, J. (1998): A new auroral feature: The nightside gap. Geophys. Res. Lett., **25**, 3747–3750.

Church, S.R. and Thorne, R.M. (1983): On the origin of plasmaspheric hiss: Ray path integrated amplification. J. Geophys. Res., **88**, 7941–7957.

Cole, K.D. (1965): Stable auroral red arc, sinks for energy of D_{st} main phase. J. Geophys. Res., **70**, 1689–1706.

Comfort, R.H., Waite, J.H., Jr. and Chappell, C.R. (1985): Thermal ion temperatures from the retarding ion mass spectrometer on DE 1. J. Geophys. Res., **90**, 3475–3486.

Comfort, R.H., Newberry, I.T. and Chappell, C.R. (1988): Preliminary statistical survey of plasmaspheric ion properties from observations by DE 1/RIMS. Modeling Magnetospheric Plasma, ed. by T.E. Moore and J.H. Waite, Jr. Washington, D.C., Am. Geophys. Union, 107–114 (Geophysical Monograph Vol. 44).

Comfort, R.H., Craven, P.D. and Richards, P.G. (1995): A modified thermal conductivity for low density plasma magnetic flux tubes. Geophys. Res. Lett., **22**, 2457–2460.

Cornwall, J.M., Coroniti, F.V. and Thorne, R.M. (1971): Unified theory of SAR arc formation at the plasmapause. J. Geophys. Res., **76**, 4428–4445.

Daglis, I. (2003): Magnetic storm-still an adequate name? Eos, **84** (22), 3 June.

Daglis, I.A. and Axford, W.L. (1996): Fast ionospheric response to enhanced activity in geospace: Ion feeding of the inner magnetotail. J. Geophys. Res., **101**, 5047–5065.

Daglis, I.A., Sarris, E.T. and Wilken, B. (1993): AMPTE/CCE CHEM observations of the energetic ion

population at geosynchronous altitudes. Ann. Geophys., **11**, 685–696.
Daglis, I.A., Thorne, R.M., Baumjohann, W. and Orsini, S. (1999): The terrestrial ring current: origin, formation, and decay. Rev. Geophys., **37**, 407–438.
Dessler, A.J. and Karplus, R. (1961): Some effects of diamagnetic ring currents on Van Allen radiation. J. Geophys. Res., **66**, 2289–2295.
De Zeeuw, D.L., Sazykin, S., Wolf, R.A., Gombosi, T.I., Ridley, A.J. and Tóth, G. (2004): Coupling of a global MHD code and an inner magnetospheric model: Initial results. J. Geophys. Res., **109**, A12219, doi: 10.1029/2003JA010366.
Ebihara, Y. and Fok, M.-C. (2004): Postmidnight storm-time enhancement of tens-of-keV proton flux. J. Geophys. Res., **109**, A12209, doi: 10.1029/2004JA010523.
Ebihara, Y., Ejiri, M., Nilsson, H., Sandahl, I., Milillo, A., Grande, M., Fennell, J.F. and Roeder, J.L. (2002): Statistical distribution of the storm-time proton ring current: POLAR measurements. Geophys. Res. Lett., **29** (20), 1969, doi: 10.1029/2002GL015420.
Ebihara, Y., Fok, M.-C., Wolf, R.A., Immel, T.J. and Moore, T.E. (2004): Influence of ionosphere conductivity on the ring current. J. Geophys. Res., **109**, A08205, doi: 10.1029/2003JA010351.
Ebihara Y., Fok, M.-C., Wolf, R.A., Thomsen, M.F. and Moore, T.E. (2005): Nonlinear impact of plasma sheet density on the ring current. J. Geophys. Res., **110**, A02208, doi: 10.1029/2004JA010435.
Erlandson, R.E. and Ukhorskiy, A.J. (2001): Observations of electromagnetic ion cyclotron waves during geomagnetic storms: Wave occurrence and pitch angle scattering. J. Geophys. Res., **106**, 3883–3895.
Escoubet, C.P., Fehringer, M. and Goldstein, M. (2001): The cluster mission. Ann. Geophys., **19**, 1197–1200.
Fejer, B.G., Spiro, R.W., Wolf, R.A. and Foster, J.C. (1990): Latitudinal variation of perturbation electric fields during magnetically disturbed periods: 1986 SUNDIAL observations and model results. Ann. Geophys., **8**, 441–454.
Fok, M.-C., Kozyra, J.U., Nagy, A.F. and Cravens, T.E. (1991a): Lifetime of ring current particles due to Coulomb collisions in the plasmasphere. J. Geophys. Res., **96**, 7861–7867.
Fok, M.-C., Kozyra, J.U., Warren, M.F. and Brace, L.H. (1991b): Seasonal variations in the subauroral electron temperature enhancement. J. Geophys. Res., **96**, 9773–9780.
Fok, M.-C., Kozyra, J.U., Nagy, A.F., Rasmussen, C.E. and Khazanov, G.V. (1993): Decay of equatorial ring current ions and associated aeronomical consequences. J. Geophys. Res., **98**, 19381–19393.
Fok, M.-C., Craven, P.D., Moore, T.E. and Richards, P.G. (1995): Ring current—plasmasphere coupling through Coulomb collisions. Cross-Scale Coupling in Space Plasmas, ed. by J.L. Horwitz *et al.* Washington, D.C., Am. Geophys. Union, 161–171 (Geophysical Monograph Vol. 93).
Fok, M.-C., Wolf, R.A., Spiro, R.W. and Moore, T.E. (2001): Comprehensive computational model of the Earth's ring current. J. Geophys. Res., **106**, 8417–8424.
Fok, M.-C., Moore, T.E., Wilson, G.R., Perez, J.D., Zhang, X.X., Brandt, P.C., Mitchell, D.G., Roelof, E. C., Jahn, J.-M., Pollock, C.J. and Wolf, R.A. (2003): Global ENA IMAGE simulations. Space Sci. Rev., **109**, 77–103.
Foster, J.C. and Burke, W.J. (2002): SAPS: A new characterization for subauroral electric fields. Eos AGU Trans., **83**, 393–394.
Foster, J.C. and Vo, H.B. (2002): Average characteristics and activity dependence of the subauroral polarization stream. J. Geophys. Res., **107**, 1475, doi: 10.1029/2002JA009409.
Fraser, B.J., Samson, J.C., Hu, Y.D., McPherron, R.L. and Russsell, C.T. (1992): Electromagnetic ion cyclotron waves observed near the oxygen cyclotron frequency by ISEE 1 and 2. J. Geophys. Res., **97**, 3063–3074.
Fraser, B.J., Singer, H.J., Hughes, W.J., Wygant, J.R., Anderson, R.R. and Hu, Y.D. (1996): CRRES Poynting vector observations of electromagnetic ion cyclotron waves near the plasmapause. J. Geophys. Res., **101**, 15331–15343.
Freeman, J.W. *et al.* (1993): Magnetospheric Specification Model Development code and Documentation. Report for USAF contract F19,628-90-K-0012, Rice University, Houston, TX.
Galperin, Y.I., Ponomarev, V.N. and Zosimova, A.G. (1974): Plasma convection in polar ionosphere. Ann. Geophys., **30**, 1–7.
Gloeckler, G. and Hamilton, D.C. (1987): AMPTE ion composition results. Physica Scripta, **T18**, 73–84.
Goldstein, J., Spiro, R.W., Reiff, P.H., Wolf, R.A., Sandel, B.R., Freeman, J.W. and Lambour, R.L. (2002):

IMF-driven overshielding electric field and the origin of the plasmaspheric shoulder of May 24, 2000. Geophys. Res. Lett., **29** (16), 1819, doi: 10.1029/2001GL014534.

Gombosi, T.I., DeZeeuw, D.L., Powell, K.G., Ridley, A.J., Sokolov, I.V., Stout, Q.F. and Toth, G. (2003): Adaptive mesh refinement for global magnetohydrodynamic simulation. Space Plasma Simulation, ed. by J. Buchner *et al.* Berlin, Springer, 247–274.

Gorbachev, O.A., Khazanov, G.V., Gamayunov, K.V. and Krivorutsky, E.N. (1992): A theoretical model for the ring current interaction with the earth's plasmasphere. Planet. Space Sci., **40**, 859–872.

Grebowsky, J.M. (1970): Model study of plasmapause motion. J. Geophys. Res., **75**, 4329–4333.

Grebowsky, J.M. and Chen, A.J. (1976): Effects on the plasmasphere of irregular electric fields. Planet. Space Sci., **24**, 689–696.

Green J.C. and Kivelson, M.G. (2004): Relativistic electrons in the outer radiation belt: Differentiating between acceleration mechanisms. J. Geophys. Res., **109**, A03213, doi: 10.1029/2003JA010153.

Green, J.L., Boardsen, S., Garcia, L., Taylor, W.W.L., Fung, S.F. and Reinisch, B.W. (2005): On the origin of whistler mode radiation in the plasmasphere. J. Geophys. Res., **110**, A03201, doi: 10.1029/2004JA 010495.

Hamilton, D.C., Gloeckler, G., Ipavich, F.M., Studemann, W., Wilken, B. and Kremser, G. (1988): Ring current development during the great geomagnetic storm of February 86. J. Geophys. Res., **93**, 14343–14355.

Harel, M., Wolf, R.A., Reiff, P.H., Spiro, R.W., Burke, W.J., Rich, F.J. and Smiddy, M. (1981): Quantitative simulation of a magnetospheric substorm, 1, Model logic and overview. J. Geophys. Res., **86**, 2217–2241.

Hill, T.W. (1974): Origin of the plasma sheet. Rev. Geophys., **12**, 379–388.

Huang, C.Y., Goertz, C.K. and Anderson, F.R. (1983): A theoretical study of plasmaspheric hiss generation. J. Geophys. Res., **88**, 7927–7940.

Hudson, M.K., Elkington, S.R., Lyon, J.G., Marchenko, V.A., Roth, I., Temerin, M. and Gussenhoven, M. S. (1996): MHD/particle simulations of radiation belt formation during a storm sudden commencement. Radiation Belts: Models and Standards, ed. by J.F. Lemaire *et al.* Washington, D.C., Am. Geophys. Union, 57–62 (Geophysical Monograph Vol. 97).

Isenberg, P.A., Koons, H.C. and Fennell, J.F. (1982): Simultaneous observations of energetic electrons and dawnside chorus in geosynchronous orbit. J. Geophys. Res., **87**, 1495–1503.

Jordanova, V.K., Farrugia, C.J., Janoo, L., Quinn, J.M., Torbert, R.B. *et al.* (1998): October 1995 magnetic cloud and accompanying storm activity: Ring current evolution. J. Geophys. Res., **103**, 79–92.

Jordanova, V.K., Farrugia, C.J., Thorne, R.M., Khazanov, G.V., Reeves, G.D. and Thomsen, M.F. (2001): Modeling ring current proton precipitation by electromagnetic ion cyclotron waves during the May 14–16, 1997, storm. J. Geophys. Res., **106**, 7–22.

Karlsson, T., Marklund, G.T., Blomberg, L.G. and Mälkki, A. (1998): Subauroral electric fields observed by the Freja satellite: A statistical study. J. Geophys. Res., **103**, 4327–4341.

Kelley, M.C., Fejer, B.G. and Gonzales, C.A. (1979): An explanation for anomalous equatorial ionospheric electric fields associated with a northward turning of the inter planetary magnetic field. Geophys. Res. Lett., **6**, 301–304.

Kennel C.F. and Petschek, H.E. (1966): Limit on stably trapped particle fluxes. J. Geophys. Res., **71**, 1–28.

Khazanov, G.V., Liemohn, M.W., Newman, T.S., Fok, M.-C. and Spiro, R.W. (2003a): Self-consistent magnetosphere-ionosphere coupling: Theoretical studies. J. Geophys. Res., **108** (A3), 1122, doi: 10.1029/2002JA009624.

Khazanov, G.V., Gamayunov, K.V. and Jordanova, V.K. (2003b): Self-consistent model of magnetospheric ring current and electromagnetic ion cyclotron waves: The 2–7 May 1998 storm. J. Geophys. Res., **108** (A12), 1419.

Kim, H.-J. and Chan, A.A. (1997): Fully relativistic changes in storm time relativistic electron fluxes. J. Geophys. Res., **102**, 22107–22116.

Kistler, L.M., Ipavich, F.M., Hamilton, D.C., Gloeckler, G., Wilken, B., Kremser, G. and Stüdemann, W. (1989): Energy spectra of the major ion species in the ring current during geomagnetic storms. J. Geophys. Res., **94**, 3579–3599.

Kozyra, J.U. and Nagy, A.F. (1991): Ring current decay-Coupling of ring current energy into the thermo-

sphere/ionosphere system. J. Geomagn. Geoelectr., **43**, Suppl., 285–297.
Kozyra, J.U., Brace, L.H., Cravens, T.E. and Nagy, A.F. (1986): A statistical study of the subauroral electron temperature enhancement using Dynamics Explorer 2 Langmuir probe observations. J. Geophys. Res., **91**, 11270–11280.
Kozyra, J.U., Shelley, E.G., Comfort, R.H., Brace, L.H., Cravens, T.E. and Nagy, A.F. (1987): The role of ring current O^+ in the formation of stable auroral red arcs. J. Geophys. Res., **92**, 7487–7502.
Kozyra, J.U., Rasmussen, C.E., Miller, R.H. and Lyons, L.R. (1994): Interaction of ring current and radiation belt protons with ducted plasmaspheric hiss 1. Diffusion coefficients and timescales. J. Geophys. Res., **99**, 4069–4084.
Kozyra, J.U., Rasmussen, C.E., Miller, R.H. and Villalon, E. (1995): Interaction of ring current and radiation belt protons with ducted plasmaspheric hiss 2. Time evolution of the distribution function. J. Geophys. Res., **100**, 21911–21919.
Kozyra, J.U., Jordanova, V.K., Horne, R.B. and Thorne, R.M. (1997a): Modeling of the contribution of electromagnetic ion cyclotron (EMIC) waves to stormtime ring current erosion. Magnetic Storms, ed. by B.T. Tsurutani *et al.* Washington, D.C., Am. Geophys. Union, 187–202 (Geophysical Monograph Vol. 98).
Kozyra, J.U., Nagy, A.F. and Slater, D.W. (1997b): High-altitude energy source(s) for stable auroral red arcs. Rev. Geophys., **35**, 155–190.
Kozyra, J.U., Jordanova, V.K., Borovsky, J.E., Thomsen, M.F., Knipp, D.J., Evans, D.S., McComas D.J. and Cayton, T.E. (1998): Effects of a high-density plasma sheet on ring current development during the November 2–6, 1993, magnetic storm. J. Geophys. Res., **103**, 26285–26306, 10.1029/98JA01964.
Lemon, C., Wolf, R.A., Hill, T.W., Sazykin, S., Spiro, R.W., Toffoletto, F.R., Birn, J. and Hesse, M. (2004): Magnetic storm ring current injection modeled with the Rice Convection Model and a self-consistent magnetic field. Geophys. Res. Lett., **31**, L21801.
Liemohn, M.W., Kozyra, J.U., Jordanova, V.K., Khazanov, G.V., Thomsen, M.F. and Cayton, T.E. (1999): Analysis of early phase ring current recovery mechanisms during geomagnetic storms. Geophys. Res. Lett., **26**, 2845–2848.
Lorentzen, KR., McCarthy, M.P., Parks, G.K., Foat, J.E., Millan, R.M., Smith, D.M., Lin, R.P. and Treilhou, J.P. (2000): Precipitation of relativistic electrons by interaction with electromagnetic ion cyclotron waves. J. Geophys. Res., **105**, 5381–5389.
Lui, A.T.Y., Elphinstone, R.D., Murphree, J.S., Henderson, M.G., Vo, H.B., Cogger, L.L., Lühr, H., Ohtani, S., Newell, P.T. and Reeves, G.D. (1995): Special features of a substorm during high solar wind dynamic pressure. J. Geophys. Res., **100**, 19095–19108.
Lyons, L.R., Thorne, R.M. and Kennel, C.F. (1972): Pitch-angle diffusion of radiation belt electrons with the plasmasphere. J. Geophys. Res., **77**, 3455–3474.
Maynard, N.C. (1978): On large poleward directed electric fields at sub auroral latitudes. Geophys. Res. Lett., **5**, 617–618.
Meredith P.N., Horne, R.B. and Anderson, R.R. (2001): Substorm dependence of chorus amplitudes: Implications for the acceleration of electrons to relativistic energy. J. Geophys. Res., **106**, 13165–13178.
Mitchell, D.G. *et al.* (2000): High energy neutral atom (HENA) imager for the IMAGE mission. Space Sci. Rev., **91**, 67–112.
Mitchell, D.G., Brandt, P.C., Roelof, E.C., Hamilton, D.C., Retterer, K. and Mende, S. (2003): Global imaging of O^+ from IMAGE/HENA. Space Sci. Rev., **109**, 63–75.
Moore, T.E. *et al.* (1999): Source processes in the high-latitude ionosphere. Space Sci. Rev., **88** (1–2), 7–84.
Moore, T.E., Fok, M.-C., Chandler, M.O., Chappell, C.R., Christon, S.P. *et al.* (2005a): Plasma sheet and (nonstorm) ring current formation from solar and polar wind sources. J. Geophys. Res., **110**, A02210, doi: 10.1029/2004JA010563.
Moore, T.E., Fok, M-C., Christon, S.P., Chen, S.-H., Chandler, M.O., Delcourt, D.C., Fedder, J., Slinker, S. and Liemohn, M. (2005b): Solar and ionospheric plasmas in the ring current. Global Physics of the Coupled Inner Magnetosphere, Wshington, D.C., Am. Geophys. Union (Geophysical Monograph) (in press).
O'brien T.P., K.R., Lorentzen, I.R., Mann, N.P., Meredith, J.B., Blake, J.F., Fennell, M.D., Looper, Milling,

D.K. and Anderson, R.R. (2003): Energization of relativistic electrons in the presence of ULF power and MeV microbursts: Evidence for dual ULF and VLF acceleration. J. Geophys. Res., **108** (A8), 1329.

Peymirat, C., Richmond, A.D. and Kobea, A.T. (2000): Electrodynamic coupling of high and low latitudes: Simulations of shielding/overshielding effects. J. Geophys. Res., **105**, 22991–23003.

Pollock, C.J. *et al.* (2001): First medium energy neutral atom (MENA) images of Earth's magnetosphere during substorm and storm-time. Geophys. Res. Lett., **28**, 1147–1150.

Rees, M.H. and Roble, R.G. (1975): Observations and theory of the formation of stable auroral red arcs. Rev. Geophys., **13**, 201–242.

Reeves, G.D., McAdams, K.L. and Friedel, R.H.W. (2003): Acceleration and loss of relativistic electrons during geomagnetic storms. Geophys. Res. Lett., **30**, 1529.

Rich, F.J., Burke, W.J., Kelley, M.C. and Smiddy, M. (1980): Observations of field-aligned currents in association with strong convection electric fields at subauroral latitudes. J. Geophys. Res., **85**, 2335–2340.

Rowland, D.E. and Wygant, J.R. (1998): Dependence of the large-scale, inner magnetospheric electric field on geomagnetic activity. J. Geophys. Res., **103**, 14959–14964.

Sandel, B.R. *et al.* (2000): The extreme ultraviolet imager investigation for the IMAGE mission. Space Sci. Rev., **91**, 197–242.

Sandel, B.R., King, R.A. Forrester, W.T. Gallagher, D.L. Broadfoot, A.L. and Curtis, C.C. (2001): Initial result from the IMAGE Extreme Ultraviolet Imager. Geophys. Res. Lett., **28**, 1439–1442.

Schulz, M. (1997): Direct influence of ring current on auroral oval diameter. J. Geophys. Res., **102**, 14149–14154.

Schunk, R.W., and Nagy, A.F. (2000): Ionospheres—Physics, Plasma Physics, and Chemistry. Cambridge, Cambridge Univ. Press.

Shawhan, S.D. (1979): Magnetospheric plasma wave research 1975–1978. Rev. Geophys. Space Phys., **17**, 705–724.

Shelley, E.G., Klumpar, D.M., Peterson, W.K., Ghielmetti, A., Balsiger, H., Geiss, J. and Rosenbauer, H. (1985): AMPTE/CCE observations of the plasma composition below 17 keV during the September 4, 1984 magnetic storm. Geophys. Res. Lett., **12**, 321–324.

Slater, D.W., Gurgiolo, C., Kozyra, J.U., Kleckner, E.W. and Winningham, J.D. (1987): A possible energy source to power stable auroral red arcs: Precipitating electrons. J. Geophys. Res., **92**, 4543–4552.

Smiddy, M., Kelly, M.C., Burke, W., Rich, F., Sagalyn, R., Shuman, B., Hays, R. and Lai, S. (1977): Intense poleward directed electric fields near the ionospheric projection of the plasmapause. Geophys. Res. Lett., **4**, 543–546.

Sonwalkar, V.S. and Inan, U.S. (1989): Lightning as an embryonic source of VLF hiss. J. Geophys. Res., **94**, 6986–6994.

Southwood, D.J. and Wolf, R.A. (1978): An assessment of the role of precipitation in magnetospheric convection. J. Geophys. Res., **85**, 5227–5232.

Spiro, R.W. and Wolf, R.A. (1984): Electrodynamics of convection in the inner magnetosphere. Magnetospheric Currents, ed. by T.A. Potemra. Washington, D.C., Am. Geophys. Union, 247–259 (Geophysical Monograph Vol. 28).

Spiro, R.W., Heelis, R.A. and Hanson, W.B. (1978): Ion convection and the formation of the midlatitude F region ionization trough. J. Geophys. Res., **83**, 4255–4264.

Spiro, R.W., Heelis, R.A. and Hanson, W.B. (1979): Rapid subauroral ion drifts observed by Atmosphere Explorer C. Geophys. Res. Lett., **6**, 657–660.

Spiro, R.W., Wolf, R.A. and Fejer, B.G. (1988): Penetration of high-latitude-electric field effects to low latitudes during SUNDIAL 1984. Ann. Geophys., **6**, 39–49.

Spitzer, L. (1962): Physics of Fully Ionized Gases, 2nd ed., chap. 5. New York, Interscience.

Stern, D.P. (1975): The motion of a proton in the equatorial magnetosphere. J. Geophys. Res., **80**, 595–599.

Strangeway, R.J., Russell, C.T., Carlson, C.W., McFadden, J.P., Ergun, R.E., Temerin, M., Klumpar, D.M., Peterson, W.K. and Moore, T.E. (2000): cusp field-aligned currents and ion outflows. J. Geophys. Res., **105** (A9), 21129.

Stüdemann, W., Wilken, B., Kremser, G., Korth, A., Fennell, J.F. *et al.* (1987): The May 2–3, 1986 magnetic

storm: First energetic ion composition observations with the MICS instrument on Viking. Geophys. Res. Lett., **14**, 455–458.

Summers, D. and Ma, C.-Y. (2000): A model for generating relativistic electrons in the Earth's inner magnetosphere based on gyroresonant wave-particle interactions. J. Geophys. Res., **105**, 2625–2639.

Summers, D. and Thorne, R.M. (2003): Relativistic electron pitch-angle scattering by electromagnetic ion cyclotron waves during geomagnetic storms. J. Geophys. Res., **108** (A4), 1143.

Thorne, R.M. and Horne, R.B. (1992): The contribution of ion-cyclotron waves to electron heating and SAR-arc excitation near the storm time plasmapause. Geophys. Res. Lett., **19**, 417–420.

Thorne, R.M., Smith, E.J., Burton, R.K. and Holzer, R.E. (1973): Plasmaspheric hiss. J. Geophys. Res., **78**, 1581–1596.

Toffoletto, F.R., Spiro, R.W., Wolf, R.A., Birn, J. and Hesse, M. (2001): Modeling inner magnetospheric electrodynamics. Space Weather, ed. by Song *et al.* Washington, D.C., Am. Geophys. Union, 265–272 (Geophysical Monograph Vol. 125).

Tsurutani, B.T. and Smith, E.J. (1977): Two types of magnetospheric ELF chorus and their substorm dependences. J. Geophys. Res., **82**, 5112–5128.

Tsyganenko, N.A. (1995): Modeling the Earth's magnetospheric magnetic field confined within a realistic magnetopause. J. Geophys. Res., **100**, 5599–5612.

Tsyganenko, N.A., Singer, H.J. and Kasper, J.C. (2003): Storm-time distortion of the inner magnetosphere: How severe can it get. J. Geophys. Res., **108** (A5), 1209, doi: 10.1029/2002JA009808.

Volland, H. (1973): A semiempirical model of large-scale magnetospheric electric fields. J. Geophys. Res., **78**, 171–180.

Van Allen, J.A. (1959): The geomagnetically trapped corpuscular radiation. J. Geophys. Res., **64**, 1683–1689.

Vasyliunas, V.M. (1970): Mathematical models of magnetospheric convection and its coupling to the ionosphere. Particles and Fields in the Magnetosphere, ed. by B. McCormac. Norwell, D. Reidel, 60–71.

Volland, H. (1978): A model of the magnetospheric electric convection field. J. Geophys. Res., **83**, 2695–2699.

Walt, M. (1996): Source and loss processes for radiation belt particles. Radiation Belts: Models and Standards, ed. by J.F. Lemaire *et al.* Washington, D.C., Am. Geophys. Union, 1–13 (Geophysical Monograph Vol. 97).

Weimer, D.R. (1995): Models of high-latitude electric potentials derived with a least error fit of spherical harmonic coefficients. J. Geophys. Res., **100**, 19595–19607.

Weimer, D.R. (2001): An improved model of ionospheric electric potentials including substorm perturbations and applications to the Geospace Environment Modeling November 24, 1996, event. J. Geophys. Res., **106**, 407–416.

Wentworth, R.C., MacDonald, W.M. and Singer, S.F. (1959): Lifetimes of trapped radiation belt particles determined by Coulomb scattering. Phys. Fluids, **2**, 499–509.

Wolf, R.A. (1970): Effects of ionospheric conductivity on convective flow of plasma in the magnetosphere. J. Geophys. Res., **75**, 4677–4698.

Wolf, R.A. (1975): Ionosphere-magnetosphere coupling. Space Sci. Rev., **17**, 537–562.

Wolf, R.A. (1983): The quasi-static (slow-flow) region of the magnetosphere. Solar Terrestrial Physics, ed. by R.L. Carovillano and J.M. Forbes. Norwell, D. Reidel, 303–368.

Wolf, R.A. (1995): Magnetospheric configuration. Introduction to Space Physics, ed. by M.G. Kivelson and C.T. Russell, Chap. 10. Cambridge, Cambridge University Press, 288–329.

Yau, A.W. and Lockwood, M. (1988): Vertical ion flow in the polar ionosphere. Modeling Magnetospheric Plasma, ed. by T.E. Moore and J.H Waite, Jr. Washington, D.C., Am. Geophys. Union, 229–244 (Geophysical Monograph Vol. 44).

Yeh, H.-C., Foster, J.C., Rich, F.J. and Swider, W. (1991): Storm time electric field penetration observed at mid-latitude. J. Geophys. Res., **96**, 5707–5721.

Zheng, Y., Fok, M.-C. and Khazanov, G.V. (2003): A radiation belt-ring current forecasting model. Space Weather, **1** (3), 1013.